Journal of Catalysis 281 (2011) 263–272

Contents lists available at ScienceDirect

Journal of Catalysis

journal homepage: www.elsevier.com/locate/jcat

Postsynthesis of mesoporous MOR-type titanosilicate and its unique catalytic properties in liquid-phase oxidations

Hao Xu, Yingtian Zhang, Haihong Wu *, Yueming Liu, Xiaohong Li, Jingang Jiang, Mingyuan He, Peng Wu *

Shanghai Key Laboratory of Green Chemistry and Chemical Processes, Department of Chemistry, East China Normal University, North Zhongshan Rd. 3663, Shanghai 200062, PR China

ARTICLE INFO

Article history:
Received 22 March 2011
Revised 9 May 2011
Accepted 9 May 2011
Available online 15 June 2011

Keywords:
Titanosilicate
Mesopore
Mordenite
Postsynthesis
Liquid-phase oxidation
TS-1

ABSTRACT

Mesoporous titanosilicate with the MOR topology, denoted as Ti-Meso-MOR, was postsynthesized from commercially available mordenite by sequential acid, alkaline, acid, and $TiCl_4$ vapor treatments, and its catalytic oxidation properties were investigated in detail in liquid-phase oxidation reactions with hydrogen peroxide as an oxidant. A controllable acid leaching was first carried out on H-mordenite (Si/Al = 7.8) to induce a partial dealumination to Si/Al = 80, which was suitable for constructing secondary mesopores by subsequent alkaline treatment. Alkaline treatment-induced desilication introduced a large number of intracrystal mesopores. Tetracoordinated Ti species were then inserted into the resultant mesoporous mordenite with a high dealumination degree (Si/Al = 145) through the gas–solid reaction with $TiCl_4$ vapor at elevated temperatures. In comparison with conventional Ti-MOR and TS-1, Ti-Meso-MOR thus prepared exhibited an improved catalytic activity in the hydroxylation of toluene and the ammoximation of cyclohexanone as well. Moreover, Ti-Meso-MOR proved to be a robust catalyst for continuous ammoximation since the mesopores minimized diffusion limitation and suppressed coke formation efficiently.

1. Introduction

The first titanosilicate of TS-1 has achieved a great success in last decades because it is capable of catalyzing efficiently the oxidation of a variety of substrates using hydrogen peroxide [1,2]. The utilization of H_2O_2 oxidation produces water as the sole byproduct, which already leads to environmentally benign chemical processes in commercial use, i.e., the hydroxylation of phenol [3] and the ammoximation of cyclohexanone [4]. In comparison with conventional non-catalytic oximation process using hydroxylamine sulfate, TS-1-catalyzed ammoximation of cyclohexanone with H_2O_2 and NH_3 produces cleanly cyclohexanone oxime, the key material in nylon-6 manufacturing industry, without coproducing any ammonium sulfate [5]. The titanosilicate/H_2O_2 system is expected to develop green processes for the production of phenol and cresols through one-pot hydroxylation of benzene or toluene [2], while conventional hydroxylation processes usually employ corrosive liquid acid like sulfuric acid as the catalyst and co-produce a large quantity of valueless waste products [6].

The liquid-phase reactions operated under mild conditions and in the presence of water (contained inevitably in aqueous H_2O_2 and coproduced during reactions) usually suffer more problems of kinetic mass transfer than the gas-phase reactions carried out at high temperatures [7]. Moreover, TS-1 with 10-membered ring (MR) window of approximately 5.5 Å in size proposes significant diffusing limitations to the large molecules penetrating into the pores [8]. Additionally, the reaction mechanism of titanosilicate/H_2O_2 catalytic system is postulated to involve the Ti–OOH species or 5-MR intermediate formed via the coordination of Ti site with H_2O_2 and solvent molecules [9]. Once these species are formed, they may narrow the kinetic size of zeolite pores obviously and then hinder the mass transfer therein. Thus, how to enhance the accessibility of substrate molecules to Ti sites turns out to be an important issue in titanosilicate catalysis. With the aim of overcoming the problems encountered by medium-pore TS-1, an alternative way is to develop titanosilicates with larger porosities. In this sense, those with 12-MR pores have been hydrothermally synthesized or postsynthesized, e.g., Ti-MWW [10], Ti-Beta [11], Ti-MTW [12], and Ti-MOR [13]. They are superior to TS-1 especially in the selective oxidation of bulky substrates. On the other hand, for the titanosilicates originating from lamellar precursors, the techniques of phase delamination [14,15], interlayer pillaring [16], and expansion [17] have been developed to improve their porosity and then oxidation ability effectively.

Among larger-pore zeolites, MOR-type aluminosilicate is hydrothermally synthesized easily even in the absence of any organic structure-directing agent, and it serves as an important solid acid catalyst that is widely used in petrochemical processes [18]. Direct synthesis of Ti-MOR, however, is still of a great challenge. This is

* Corresponding authors. Fax: +86 21 6223 2292.
E-mail addresses: hhwu@chem.ecnu.edu.cn (H. Wu), pwu@chem.ecnu.edu.cn (P. Wu).

0021-9517/$ - see front matter © 2011 Elsevier Inc. All rights reserved.
doi:10.1016/j.jcat.2011.05.009

because its specific structure features such as 4-MR make the crystallization of MOR structure impossible under siliceous conditions, let alone in the absence of any alkali source, a critical precondition favored by titanosilicate. Ti-MOR is thus prepared by combined postsynthesis treatments including dealumination and $TiCl_4$ vapor treatment [13]. It is shown to be more active than TS-1 in the hydroxylation of aromatics [19]. However, the one-dimensional (1D) channel system of Ti-MOR is short of interconnectivity, which may make it lack the potential activity possessed by the zeolites with three-dimensionally connected channels. Introducing intercrystal and/or intracrystal mesopores into Ti-MOR are thus expected to minimize the diffusion limitation possibly.

Several techniques have been established to create extra mesopores in microporous zeolite crystals, such as post-treatments of acid leaching [20] or base leaching [21], and direct synthesis with hard [22] or soft templates [23]. All these methods are sorted into two categories, that is, templating and non-templating ways. With respect to templating way, both soft templates of supramolecular organics [23–26] and hard templates of carbon nanoparticles [27], polymer [28], starch [29], and resins [30] have been used successfully to induce mesopores into zeolite crystals during hydrothermal synthesis processes.

As for non-templating route, the nucleation and crystal growth are controlled in synthesis process, which leads to self-assembling of primary particles and formation of intercrystal mesopores [31]. Another feasible approach is to carry out demetallation including streaming, acid, and base treatments. Low silica zeolites are usually steamed and then treated with acid to generate mesoporosity via dealumination process. For example, USY, the main active component in FCC catalysts, is commercially produced in this way for decades.

For high silica zeolites (Si/Al > 5), alkaline treatment-induced desilication is powerful for creating extra mesopores [32]. However, the leaching of silicon from the structures closely depends on the treatment conditions, e.g., concentration of alkaline solution, temperature, and time [33,34]. Moreover, the aluminum content of zeolites alters the desilication process, and the Al content suitable for mesopore formation is reported to be in the Si/Al ratio range of 20–50 in the case of ZSM-5 zeolite [35]. This technique has been applied widely to the preparation of other mesoporous zeolites such as mordenite (MOR) [36], zeolite Y (FAU) [37], β zeolite (BEA) [38], ZSM-22 (MTW) [39], and SSZ-13 (CHA) [40]. Up to date, the researches predominately focus on the design of solid acid catalysts with larger porosities but rarely deal with the preparation of metallosilicates with unique redox properties.

In this study, mesopores have been introduced into MOR crystals to improve the accessibility to Ti active sites and then oxidation activity. The catalytic performance of postsynthesized Ti-Meso-MOR has been compared with that of conventional Ti-MOR and TS-1 in the hydroxylation of toluene and the ammoximation of cyclohexanone.

2. Experimental

2.1. Zeolite materials

A commercially available H-mordenite with a Si/Al molar ratio of 7.8 was purchased from Shangsi Fine Chemical Co., China. Denoted as Parent-MOR, it was used as-received as the starting material for preparing dealuminated MOR with or without mesopores.

Parent-MOR was first refluxed in 6 M HNO_3 solution at a liquid-to-solid ratio of 1:50 w/w for 20 h. The treated sample was subsequently filtrated and washed with deionized water until the pH value of the filtrate was over 5. It was then dried at 353 K overnight and further calcined in air at 973 K for 10 h to obtain a partially dealuminated sample (Acid-MOR) with a Si/Al ratio of 80. This sample was subjected to acid refluxing again with 6 M HNO_3 for 20 h following conventional dealumination procedures reported previously [41], which gave a deeply dealuminated sample (C-MOR, Si/Ai = 195).

Alkaline treatment was performed on Acid-MOR to generate mesopores. Following a literature procedure [42], Acid-MOR (9 g) was treated in 270 mL NaOH solution (0.2 M) at 338 K for 0.5 h. The sample was collected by centrifugation, washed with deionized water repeatedly until the pH value reached ca. 7, and finally dried at 353 K overnight. The solid product yield after desilication corresponded to 70.5 wt.%. Then, another acid treatment (6 M HNO_3, refluxing for 20 h) was carried out on the alkaline-treated sample. The ion-exchange into proton form and removal of Al from the framework occurred simultaneously during this process, leading to dealuminated Meso-MOR (Si/Al = 145).

2.2. Preparation of titanosilicates

Ti-containing MOR samples were postsynthesized through a solid–gas reaction between dealuminated MOR and $TiCl_4$ vapor at elevated temperatures [13]. A dealuminated MOR sample (2.0 g) placed in a quartz tube reactor (i.d. 4 cm) was pretreated at 773 K for 2 h in a dry N_2 stream (30 mL min^{-1}). Then, the reactor was brought to a treatment temperature of 673 K, where the N_2 stream went through an anhydrous $TiCl_4$ solution contained in a glass bubbler and maintained at 303 K. The $TiCl_4$ vapor saturated in N_2 flow was carried into the reactor to contact the zeolite bed for a determined period of time. After the treatment, the sample was purged with pure N_2 at the same temperature for 1 h to remove any residual $TiCl_4$ from the zeolite powder. After cooling to room temperature in N_2, the treated sample was washed with deionized water under stirring until chloride ions were not detected in the filtrate by $AgNO_3$ solution. The sample was then dried in air at 353 K overnight. The duration of $TiCl_4$ treatment was varied in the range of 5 min^{-1} h to achieve different Ti incorporation. The Ti-containing samples obtained from Meso-MOR and C-MOR were denoted as Ti-Meso-MOR and Ti-MOR, respectively. Scheme 1 shows graphically the whole procedures for preparing Ti-Meso-MOR.

For control experiment, TS-1 was hydrothermally synthesized from raw materials of tetraethyl orthosilicate (TEOS), tetrabutyl orthotitanate (TBOT), and tetrapropylammonium hydroxide (TPAOH) solution following typical ENI method [43]. The synthetic gel was prepared to have a molar composition of 0.18TPAOH:0.01 or $0.03TiO_2$:$1.0SiO_2$:$18H_2O$. The gels were transferred into a 120-mL Teflon-lined autoclave and crystallized at 443 K for 3 days under rotation (100 rpm). The two TS-1 samples were recovered by filtration, washed thoroughly by deionized water, dried at 353 K, and calcined in air at 823 K for 10 h, which had Si/Ti ratios of 95 and 35.

2.3. Characterization methods

Powder X-ray diffraction (XRD) was employed to check the structure and crystallinity of the zeolites. The XRD patterns were collected on a Rigaku Ultima IV diffractometer using Cu Kα radiation at 35 kV and 25 mA in the 2θ angle range of 5–35°. Scanning electron microscopy (SEM) was performed on a Hitachi S-4800 microscope to determine the morphology. Transmission electron microscopy (TEM) images were collected on a JEOL JEM-2100 microscope after the samples were deposited onto a holey carbon foil supported on a copper grid. The Ti and Al contents were determined by inductively coupled plasma emission spectrometry (ICP) on a Thermo IRIS Intrepid II XSP atomic emission spectrometer

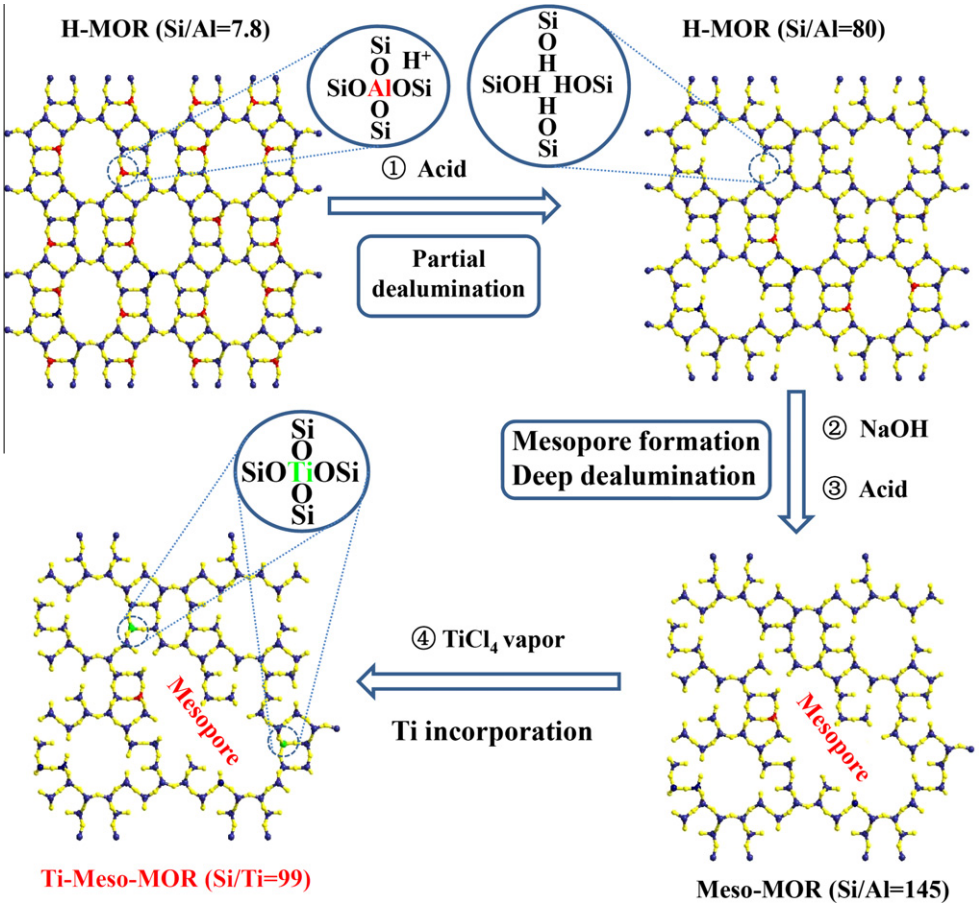

Scheme 1.

after dissolving the samples in HF solution. The specific surface area, pore volume, and pore size distribution was measured by N_2 adsorption at 77 K on a BELSORP-MAX instrument equipped with a precise sensor for low pressure measurement. The samples were activated at 573 K under vacuum for at least 10 h. The micropore size distribution was determined using Saito–Foley (SF) method. The mesopore size distribution was determined by Barett–Joyner–Halenda (BJH) method from the desorption branches of the isotherms. The UV–visible diffuse reflectance spectra were recorded on a Shimadzu UV-2550 spectrophotometer using $BaSO_4$ as a reference. The IR spectra were collected on Nicolet Nexus 670 FT-IR spectrometer in absorbance mode at a spectral resolution of 2 cm^{-1} using KBr technique (2 wt.% wafer). The ^{29}Si MAS NMR spectra were measured on a VARIAN VNMRS 400WB NMR spectrometer at a frequency of 79.43 MHz using one-pulse method, a spinning rate of 3 kHz, a recycling delay of 60 s. The chemical shift was referred to Q_8M_8 ($[(CH_3)_3SiO]_8SiO_{12}$). Thermogravimetry (TG) and derivative thermogravity (DTG) analyses were carried out on a Mettler TGA/SDTA 851^e instrument with a ramping rate of 10 K min^{-1} in an air flow of 40 mL min^{-1}.

2.4. Catalytic reactions

The hydroxylation of toluene with H_2O_2 was carried out in a 50-mL flask reactor equipped with a condenser. In a typical run, the mixture of 0.05 g catalyst, 10 g toluene, and 1 g H_2O was stirred vigorously at 363 K. Then, 10 mmol H_2O_2 (30 wt.%) was added into the reactor to start the hydroxylation. After the reaction was carried out for a desirable period of time (1–5 h), 20 mL ethanol was added to homogenize the organic phase and the aqueous phase. The products were analyzed on a gas chromatograph (GC9800, FAAP capillary column) and quantified using chlorobenzene as an internal standard.

The ammoximation of cyclohexanone was first carried out in a batchwise reactor using water of *tert*-butanol (85 wt.% aqueous solution) as a solvent. The mixture of catalyst (0.05–0.3 g), 20 mmol cyclohexanone, and 12 g solvent (*t*-BuOH or H_2O) were heated in a 50-mL flask to 333 K, where H_2O_2 and $NH_3{\cdot}H_2O$ were added to initiate the reaction for 0.5 or 2 h. The molar ratio of NH_3:H_2O_2:cyclohexanone was 1.5:1.2:1. The ammoximation was further carried out in a slurry bed reactor continuously to evaluate the catalyst life. The glass slurry reactor (160 mL) was equipped with a glass sand filter and a magnetic stirrer. A desirable amount of catalyst powder (1.6 g) was dispersed in 120 mL *t*-BuOH solution (85 wt.%) in the reactor. After the temperature reached 345 K, the mixture of cyclohexanone and *t*-BuOH (weight ratio of 1:2.94) and 30 wt.% H_2O_2 were fed into the reactor separately with micropumps. Meanwhile, ammonia gas (99.9%) was charged into the reaction system with a mass flowmeter at a constant rate of 145 mL min^{-1}. The feeding rate of cyclohexanone/*t*-BuOH mixture was kept constant at 96 mL h^{-1}, which corresponded to a feeding rate of 21.8 mL h^{-1} for cyclohexanone. The molar ratios of H_2O_2/ketone and NH_3/ketone were maintained constantly at 1.1:1 and 1.7:1, respectively. When the reactants were added continuously into the reactor, the reaction mixture overflowed from the outlet filter, while the catalyst remained inside. The organic products at

different intervals were analyzed on GC to obtain the conversion of cyclohexanone and the selectivity of oxime.

3. Results and discussion

3.1. Synthesis and characterization of MOR-type titanosilicates

The structural change of mordenite after various treatments was first investigated with X-ray diffractometer (XRD). Fig. 1 shows the XRD patterns of Parent-MOR together with those of post-treated samples. The samples were characteristic of a typical MOR topology, and possessed the diffractions very comparable in intensity. Mordenite was previously verified to be capable of bearing thermal treatment at 973 K and refluxing in concentrated acid solution because of a high silica nature. A deep dealumination to an extremely low Al content was thus realized by repeated thermal and acid treatments but without destruction of the crystalline structure [41]. Alkaline treatment prefers desilication to alumination, which may cause structural degradation easily under severe conditions of concentrated NaOH solution. Nevertheless, controlled alkaline treatment may sharpen the XRD peaks by dissolving amorphous parts more easily than crystalline zeolite [44]. Likewise, we carried out the desilication of mordenite under controlled conditions. The sample was pre-dealuminated to a reasonable Si/Al ratio of 80 and then subjected to alkaline treatment using a dilute NaOH solution (0.2 M) at 338 K for a short period of 0.5 h. Thus, the observed diffraction peaks of resultant Meso-MOR were slightly sharper than Parent-MOR in the 2θ range of 5–10° (Fig. 1c). This indicates that the combined acid, thermal, and base treatments did impose structural change on the framework of mordenite at least at a micrometer scale. After incorporation of Ti species into dealuminated moredenite samples by $TiCl_4$ vapor treatment at 673 K, both Ti-MOR and Ti-Meso-MOR showed almost the same XRD patterns as Fig. 1, apparently with preservation of the structural order of mordenite (XRD patterns not shown).

The N_2 adsorption–desorption isotherms of the samples are depicted in Fig. 2. Both Ti-MOR and Ti-Meso-MOR still showed the same type IV isotherms as Parent-MOR irrespective of dealumination, desilication, or titanation treatments. In agreement with previous report [41], the dealumination slightly increased the adsorption capacity by creating new pores or cavity within crystals (Fig. 2b). A controlled alkaline treatment made the adsorption capacity increase further although not significantly as a result of removing a part of silica from the framework (Fig. 2c). The enlarged isotherms indicated that the samples possessed hysteresis loops at

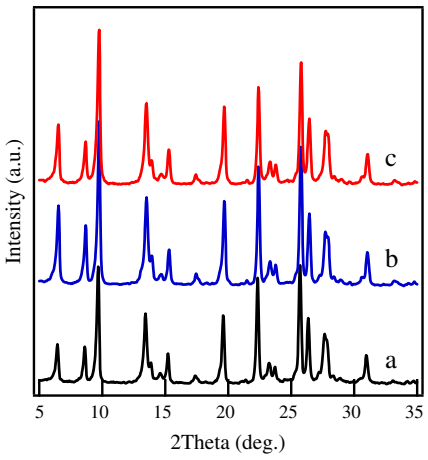

Fig. 1. XRD patterns of Parent-MOR (a), conventionally dealuminated MOR (b), and Meso-MOR (c).

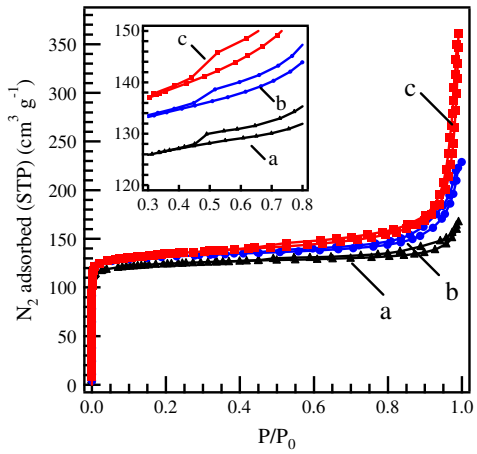

Fig. 2. N_2 adsorption and desorption isotherms of Parent-MOR (a), Ti-MOR (b), and Ti-Meso-MOR (c). The insets show the region of multilayer adsorption.

P/P_0 of 0.4–0.8 with Ti-Meso-MOR most notably. This suggests the presence of newly formed mesopores. More obvious difference in N_2 uptake was observed in the region of higher relative pressure. In comparison with Parent-MOR and Ti-MOR, Ti-Meso-MOR showed greatly enhanced N_2 adsorption at P/P_0 = 0.9–0.99 (Fig. 2c), suggesting the alkaline treatment was conductive to generating the pores with larger dimensions, probably corresponding to intercrystal mesopores. As shown by below SEM images, the mordenite samples were of micrometer-sized secondary particles consisting of smaller primary particles. The alkaline treatment may dissolve easily the silicate species that connected the primary nanocrystals to create this kind of large intercrystal pores in addition to the intracrystal mesopores formed as a result of desilication within primary particles.

The pore size distribution curves were calculated for micropore and mesopore with SF method and BJH method, respectively (Fig. 3). Both Parent-MOR and post-treated samples showed a narrow peak at ca. 0.6 nm, in accordance with the 12-MR channels of mordenite since the post-treatments especially the desilication did not destroy the structure of micropores. In the distribution region of mesopore, the curve of Ti-MOR was almost the same as Parent-MOR, but had a weak peak at 10–30 nm, which was probably contributed by secondary pores. Actually, the secondary pores were previously demonstrated to be created by acid treatment as a result of dealumination [45]. However, different from the Parent-MOR and Ti-MOR samples, Ti-Meso-MOR showed a more notable distribution in the range of 10–100 nm (Fig. 3c), indicating the presence of mesopores. Apparently, the desilication by alkaline

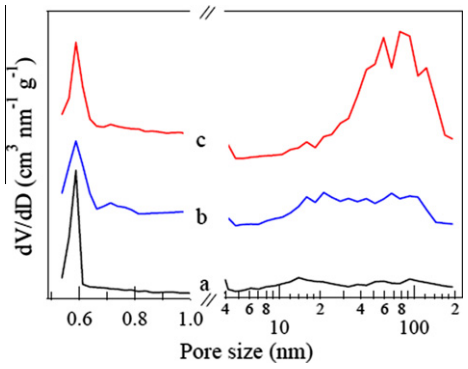

Fig. 3. Pore size distribution of Parent-MOR (a), Ti-MOR (b), and Ti-Meso-MOR (c).

treatment was more efficient than dealumination in terms of mesopore formation.

The specific surface area and pore volume are given together with the chemical compositions determined by ICP analysis in Table 1. The harsh acid treatments repeatedly carried out on Parent-MOR caused a deep dealumination, which increased greatly the Si/Al ratio for Ti-MOR and Ti-Meso-MOR (Table 1, Nos. 1–3). Meanwhile, the total surface area and the pore volume of mesopores or secondary pores increased after the aluminum ions were eliminated extensively. Among three samples, Ti-Meso-MOR, the preparation processes of which included the alkaline treatment, possessed the largest $S_{Langmuir}$, V_{total}, and V_{meso} as a result of forming more mesopores. Its V_{micro} was the smallest, implying the possibility of generating mesopores at the expense of destruction of a part of micropores. However, the amount of micropores vanished was far below the mesopore volume increased. A large number of mesopores were thus presumably created in intracrystal spaces as evidenced by SEM and TEM images (see next paragraph).

Fig. 4 shows the SEM micrographs with different magnification for Parent-MOR and two postsynthesized samples. The samples were composed of the crystals with a morphology of rectangular column (1×0.2 μm). Both the morphology and the crystal size were intact after dealumination and desilication treatments. The crystals of Parent-MOR showed very smooth and distinct surface and outline (Fig. 4a and b). Sequential acid treatments did not alter the crystal surface obviously (Fig. 4c and d). The dealumination only made the edges and corners of crystals worn to a very limited degree. Considering the fact that Al ions were all isolated and tetrahedrally coordinated in the framework, the removal of Al ions taking place at an atomic level reasonably would cause no visible micrometer-scale change to the crystals. On the other hand, many grooves and voids appeared on the crystal surface of Ti-Meso-MOR (Fig. 4e and f). This should be due to dissolving a part of silica species from the zeolite framework in alkaline treatment. The alkaline corrosion created randomly the voids more than 20 nm in size. Nevertheless, the whole crystal shapes were not changed as a result of maintaining the mordenite structure, which was consistent with the conclusions derived from XRD.

TEM images shown in Fig. 5 gave more solid evidence for the presence of abundant mesopores in Ti-Meso-MOR. Both Parent-MOR and conventional Ti-MOR showed stripped channels corresponding to the 12-MR micropores of moredenite (Fig. 5a and b). The channels were arrayed in a highly ordered manner without any interruption, and the domain contrast of the images also implied that the crystals were almost free of unconnected region. Intracrystal mesopores thus were hardly generated during dealumination process by acid treatment. In contrast, the TEM images that were taken along different crystallographic planes and with various magnifications showed that Ti-Meso-MOR possessed a large number of white spots with dimensions more than 20 nm (Fig. 5c–f). This visualized the presence of mesopores as interruptions of the lattice planes. Disordered in pore size and shape, these mesopores existed randomly throughout different planes. In agreement with above SEM and N_2 adsorption investigations, the TEM images verified clearly that alkaline treatment developed a large quantity of intracrystal mesopores in mordenite crystals. The formation of mesopores interrupted the continuity of original micropore channels, but made them interconnected with each other. Meanwhile, it was reported that the mesopore formation started close to the external surface area and progressed toward the center of the crystals [36]. This would shorten the diffusion pathway for the molecules diffusing from outside into the micropores, maximize the mass transport through the crystals, and finally improve the accessibility to the active sites located in the pores.

Following previously well-established procedures [13], we conducted the incorporation of Ti ions into the framework of mordenite by atom-planting treatment using $TiCl_4$ vapor. The existing states of the Ti species introduced were first investigated by IR spectroscopy. Titanosilicates are all characteristic of an IR band at approximately 960 cm^{-1} irrespective of crystalline structure, which is taken as an important evidence for the presence of tetrahedral Ti species [1,2]. As shown in Fig. 6, both Ti-MOR and Ti-Meso-MOR showed the typical band at 960 cm^{-1} that is probably attributed to the Si–O–Ti stretching. The band intensity increased with prolonging the process time of $TiCl_4$ treatment, that is, increasing amount of incorporated Ti. The amount of Ti incorporated almost leveled off after the treatment for 1 h. Compared at a fixed treatment time of 1 h, the 960 cm^{-1} band of Ti-Meso-MOR was slightly more intensive that Ti-MOR (Fig. 6e), suggesting the presence of mesopores is favorable for incorporating more Ti species into mordenite structure. As depicted in Table 1, the saturated Ti incorporation corresponded to Si/Ti ratio of 99 and 115 for Ti-Meso-MOR and Ti-MOR, respectively. The $TiCl_4$ vapor molecules with a relatively bulky dimension (6.7 Å) may suffer diffusion difficulty when entering into the 12-MR channels of mordenite. However, this kind of limitation is considered to be eliminated slightly by the presence of mesopores.

UV–visible spectroscopy was applied to characterize further the coordination states of the Ti species incorporated. Both Ti-MOR and Ti-Meso-MOR showed a dominated band at approximately 220 nm (Fig. 7), which is assigned to the ligand-to-metal charge transfer from O^{2-} to Ti^{4+}. This band is usually observed for a variety of Ti-substituted zeolites, and it is characteristic of tetrahedrally coordinated Ti highly dispersed in the framework [46]. Moreover, no obvious band was observed around 330 nm due to anatase phase. In agreement with IR spectra, the results verified that the Ti species were incorporated into the silica matrix in a highly dispersed manner but not as aggregated phase, probably isolated in the framework of mordenite.

With respect to the Ti incorporation mechanism, we once addressed that the Ti species inserted to the hydroxyl nests through the reaction of one $TiCl_4$ molecule with four internal silanol groups on the basis of isotope exchange with $C^{18}O_2$ [13]. Here, ^{29}Si MAS NMR spectra were measured to take insight into this issue. As shown in Fig. 8, two resonances observed at −112 ppm

Table 1
Textural properties of different mordenite samples.

No.	Sample	Si/Al[a] ratio	Si/Ti[a] ratio	SA[b] ($m^2 g^{-1}$)	Pore volume ($cm^3 g^{-1}$)		
					V_{total}	V_{micro}[c]	V_{meso}
1	Parent-MOR	7.8	–	535	0.254	0.187	0.067
2	Ti-MOR	195	115	565	0.346	0.179	0.167
3	Ti-Meso-MOR	145	99	599	0.542	0.173	0.369

[a] Given by ICP.
[b] Specific surface area (Langmuir) given by N_2 adsorption at 77 K.
[c] Calculated from *t*-plot.

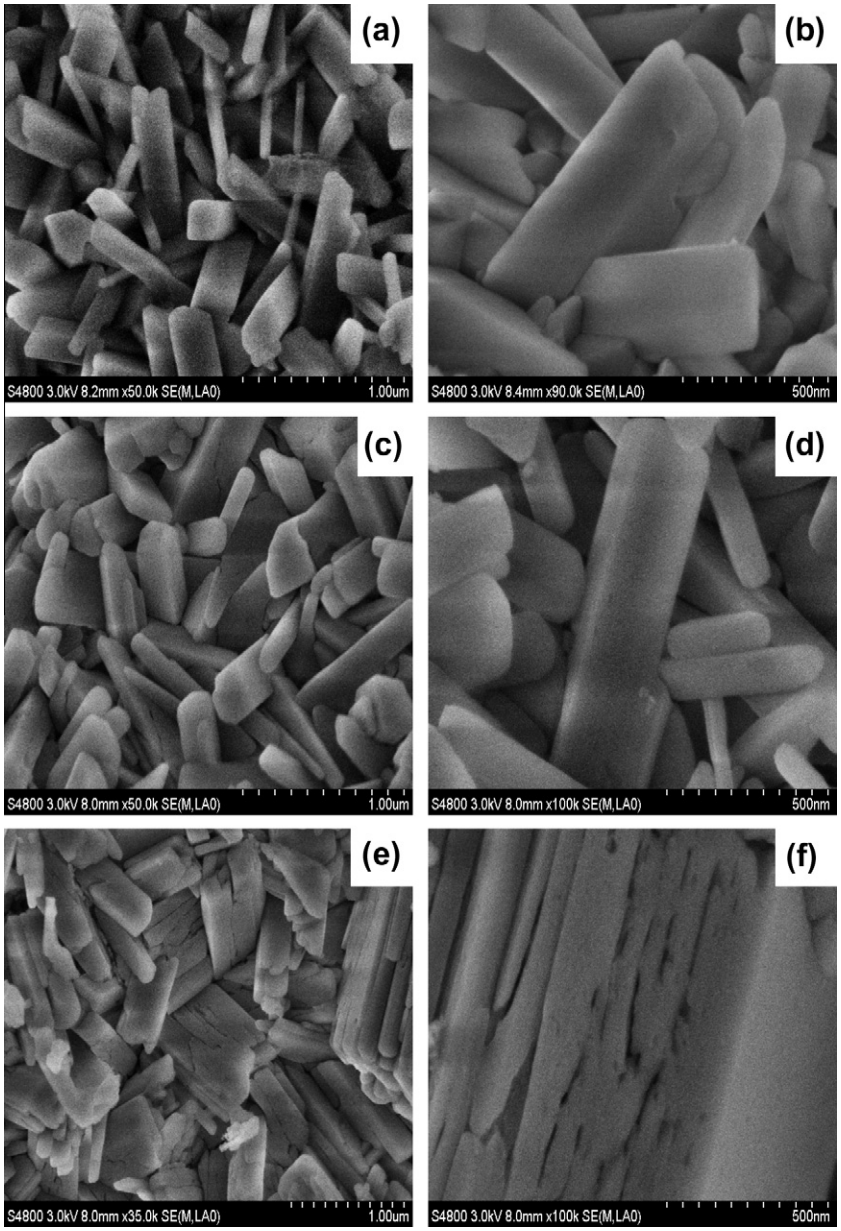

Fig. 4. SEM micrograph images of Parent-MOR (a and b), Ti-MOR (c and d), and Ti-Meso-MOR (e and f).

and −115 ppm were attributed the Q^4 groups in $Si(SiO)_4$ configuration [47]. With a comparable intensity, they were caused by overlap of four crystallographically non-equivalent tetrahedral $Si(SiO)_4$ sites. The combined acid and alkaline treatments removed the Al ions from the framework extensively and developed a broad resonance around −103 ppm (Fig. 8a). This resonance was greatly enhanced by means of ^1H–^{29}Si cross-polarization technique (Fig. S1). Thus, this resonance is reasonably assigned to the Q^3 groups of silicon-bearing OH groups, i.e., internal $Si(OH)(SiO)_3$ [48]. The Q^3 resonance was developed not intensively as expected, since the silicon ions in neighborhood may migrate into Al-deficient vacancies especially during thermal treatment process, which then eliminates a part of potential silanols [41]. As depicted in Fig. 8b, Ti-Meso-MOR possessed a less intensive Q^3 resonance than Meso-MOR, suggesting the interaction of $TiCl_4$ molecules with SiOH groups. Thus, Ti-Meso-MOR was prepared in a similar way to the titanation mechanism investigated previously for conventional dealuminated mordenite [13], but involving an additional step for developing mesopores. The desilication that occurred unselectively throughout zeolite crystals would give rise to both intracrystal mesopores and intercrystal mesopores. With respect to the specific case of intracrystal dealumination, desilication, and Ti-insertion, Scheme 1 graphically illustrates the procedures employed in the postsynthesis of Ti-Meso-MOR.

3.2. Catalytic properties of Ti-Meso-MOR in liquid-phase oxidations

3.2.1. Hydroxylation of toluene

Ti-MOR catalyst has already been shown to be more active than TS-1 zeolite in the hydroxylation of aromatics because of a large porosity of mordenite zeolite [19]. The oxidations are believed to be catalyzed by the framework Ti atoms inside zeolite pores. Moreover, the reactions are considered to take place via intermediates of Ti-peroxo species that may propose diffusion problem and transition-state shape selectivity for substrate molecules especially with bulky dimensions [1,2]. Thus, there is still room to improve

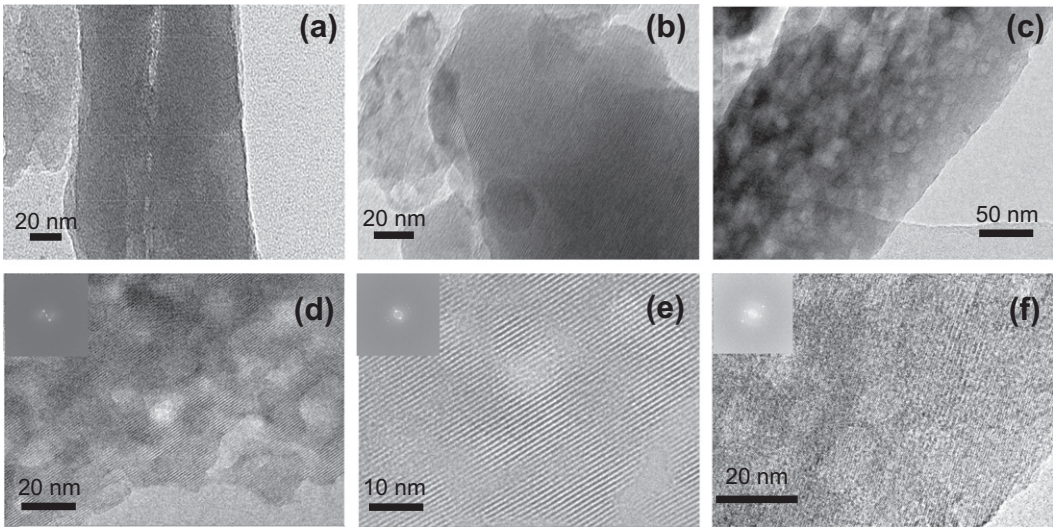

Fig. 5. TEM micrograph images of Parent-MOR (a), Ti-MOR (b), and those of Ti-Meso-MOR taken with different magnifications (c–f).

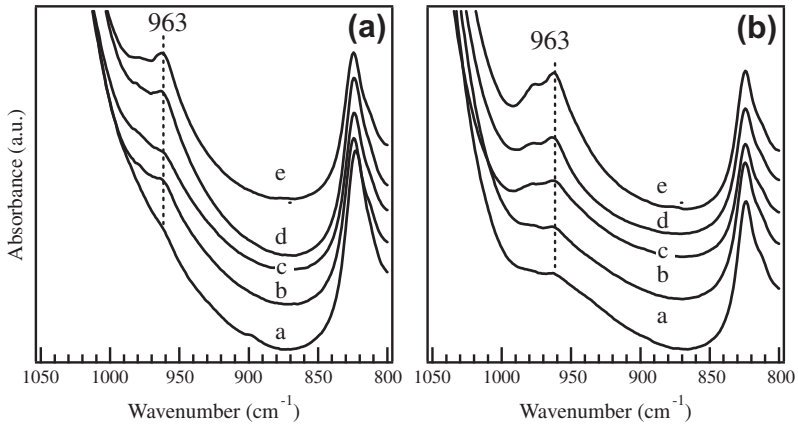

Fig. 6. IR spectra of (A) Ti-MOR and (B) Ti-Meso-MOR samples prepared by $TiCl_4$ treatment at 673 K for 5 min (a), 10 min (b), 20 min (c), 0.5 h (d), and 1 h (e).

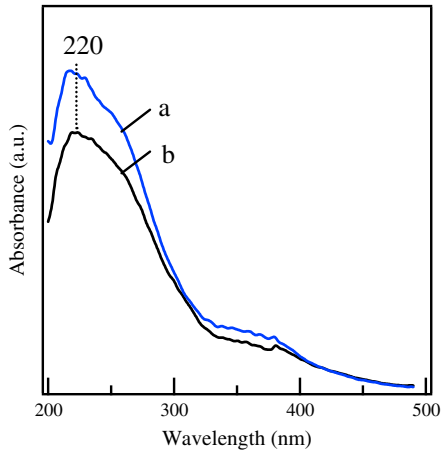

Fig. 7. UV–visible spectra of Ti-MOR (Si/Ti = 115) (a) and Ti-Meso-MOR (Si/Ti = 99) (b).

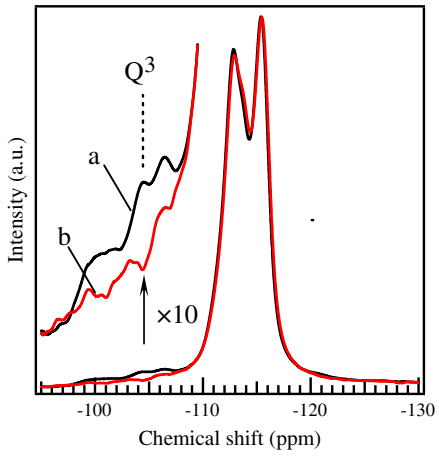

Fig. 8. ^{29}Si MAS NMR spectra of Meso-MOR (a) and Ti-Meso-MOR (b). The insets show the enlarged region of Q^3 resonance.

the catalytic performance of Ti-MOR in processing large molecules. We have compared the catalytic activity in toluene hydroxylation with H_2O_2 among TS-1, Ti-MOR, and Ti-Meso-MOR. Three samples contained similar Ti contents (Si/Ti = 95–115). Fig. 9 shows the time course of specific activity per Ti site, i.e., turnover number (TON). The TON increased rapidly with reaction time at initial stage and then turned to deactivate gradually after 1 h. Cresols formed as a result of hydroxylation of toluene were main products in which the selectivity for *para*-isomer was >60%. The reaction rate of

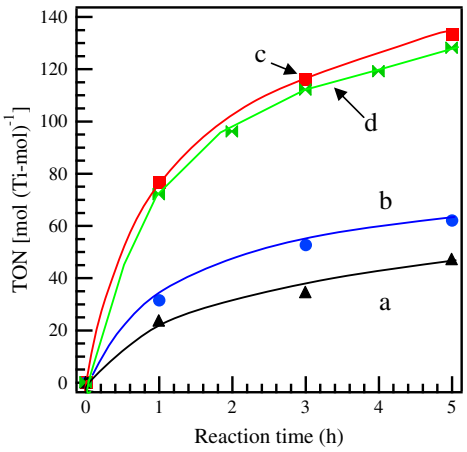

Fig. 9. The catalytic activity of toluene hydroxylation over TS-1 (a), Ti-MOR (b), Ti-Meso-MOR (c), and Ti-Meso-MOR after five reuses (d). Reaction conditions: cat., 0.05 g; toluene, 10 g; water, 1 g; H_2O_2 (30 wt.%), 10 mmol; temp., 363 K. The used catalyst was activated by calcination in air at 773 K for 5 h.

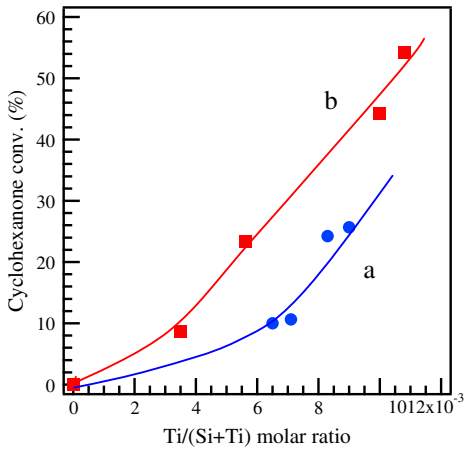

Fig. 10. Dependence of ammoximation conversion on the Ti content of Ti-Meso-MOR (a) and Ti-MOR (b). Ammoximation conditions: cat., 0.05 g; cyclohexanone, 20 mmol; ketone:H_2O_2:NH_3 = 1:1.2:1.5 (molar ratio); water, 12 g; temp., 333 K; time, 0.5 h.

Ti-MOR was slightly higher than TS-1 (Fig. 9a and b), which was accordance with the literature [49]. Different from TS-1 with three-dimensionally interconnected 10-MR channels, Ti-MOR has only one-dimensional channels but larger in pore window (12-MR). Thus, the absolute pore size of titanosilicate is crucial to its catalytic activity for bulky molecules. On the other hand, Ti-Meso-MOR showed an activity that was almost twice that of Ti-MOR (Fig. 9c).

As the substrate investigated on three catalysts was the same, the observed catalytic activity should be closely correlated to their pore sizes. With a hierarchical pore structure, Ti-Meso-MOR possessed larger specific surface area and mesopore volume than Ti-MOR zeolite. The mesopores derived from alkaline treatment are probably connected to the outside of crystals and interconnected with the micropores as well [36]. This would shorten the diffusion path for toluene molecules approaching to the Ti sites inside the pores, which contributes to an improved catalytic performance. The used Ti-Meso-MOR catalyst was regenerated by calcination in air at 773 K for 5 h and was subjected to toluene hydroxylation again under the same conditions. The activity was retained after five cycles (Fig. 9d). ICP analysis indicated that the Si/Ti ratio of the recovered catalyst was 105 after fifth reuse in toluene hydroxylation. Comparing with the Si/Ti ratio of 99 for fresh Ti-Meso-MOR, the Ti leaching accounted for only 5.7%. These results indicate that Ti-Meso-MOR is a robust and reusable oxidation catalyst. With respect to Ti leaching, even TS-1 was shown to be unstable in the epoxidation of crotyl alcohol, because the triol byproducts may chelate the Ti sites, thereby cleaving easily the Si–O–Ti bonds [50]. It seems that this kind of byproduct-induced Ti leaching was negligible in the hydroxylation of toluene with Ti-Meso-MOR.

3.2.2. Ammoximation of cyclohexanone

The advantages of introducing mesopores into titanosilicates were further demonstrated in ammoximation of cyclohexanone with ammonia and hydrogen peroxide. The cyclohexanone oxime product is the raw material for producing ε-caprolactam, an important intermediate for nylon-6 synthesis. In addition to TS-1 [51] and Ti-MWW [52], Ti-MOR also proves to be an efficient catalyst for this reaction [53]. We first checked whether or not Ti-Meso-MOR was more efficient for this reaction using a batch-type reactor. Fig. 10 compares the conversion of cyclohexanone between Ti-Meso-MOR and Ti-MOR with different Ti contents. In order to differ any variation, we have carried out the reactions using a relative low ratio of catalyst to ketone. The reactions gave cyclohexanone oxime as main product produced at >99% selectivity. The conversion of cyclohexanone increased reasonably with increasing Ti/(Si + Ti) ratio. Obviously, Ti-Meso-MOR was superior to Ti-MOR in catalytic activity. The ammoximation are believed to occur in two steps, that is, *in situ* formation of hydroxylamine via catalytic oxidation of NH_3 by H_2O_2 on Ti sites and oximation of ketone with hydroxylamine to corresponding oxime [53,4c]. Since the second step of oximation is a non-catalytic reaction, it occurs possibly even in liquid phase unless hydroxylamine formed inside the zeolite pores diffuses to outside. Thus, different to other oxidation reactions, the ketone molecules are not always necessary to enter into the zeolite channels to terminate the ammoximation reaction. Nevertheless, considering the fact that the intermediate of hydroxylamine is unstable and decomposed easily, the whole reaction could be enhanced if cyclohexanone molecules diffuse into the pores rapidly and react with hydroxylamine formed therein immediately before non-productive decomposition occurs. Of course, when the hydroxylamine molecules diffuse smoothly out of the pores and reach the ketone molecules existing in liquid phase, the ammoximation would also be helpful. The mesopores in Ti-Meso-MOR are beneficial for the hydroxylamine molecules diffusing outside and also useful for the cyclohexanone molecules approaching easily to the Ti sites inside the pores. This would lead to its higher performance of in ammoximation of cyclohexanone.

TS-1 is a highly efficient catalyst for ammoximation of cyclohexanone. The processes based on TS-1 have already been commercialized for the clean production of cyclohexanone oxime. TS-1 is capable of catalyzing the reaction almost stoichiometrically, giving ketone conversion and oxime selectivity over 95% and 99%, respectively. The performance, however, depends greatly on the reaction conditions such as relative amount of used catalyst and solvent. As shown in Table 2, both Ti-Meso-MOR and Ti-MOR were more effective than TS-1, whenever H_2O or *t*-BuOH/H_2O was used as solvent. Ti-Meso-MOR gave a ketone conversion of >95% at 99.3% oxime selectivity in both H_2O and *t*-BuOH/H_2O system, whereas the conversion of cyclohexanone reached >95% over Ti-MOR only in the co-solvent of *t*-BuOH and water. On the other hand, the reaction over TS-1 did not reach the same level as Ti-MOR and Ti-Meso-MOR unless a larger quantity of TS-1 catalyst (0.3 g) was employed.

Although above results obtained with a batch-type reactor already indicated that Ti-Meso-MOR is potentially applicable to the process of cyclohexanone ammoximation, its stability and

Table 2
A comparison of ammoximation of cyclohexanone between Ti-Meso-MOR, Ti-MOR, and TS-1.

Catalyst	Solvent	Amount of cat. (g)	Ketone conv. (%)	Oxime sel. (%)
Ti-Meso-MOR	H_2O	0.1	95.2	99.3
	t-BuOH/H_2O (85%)	0.1	97.7	99.3
Ti-MOR	H_2O	0.1	84.1	99.7
	t-BuOH/H_2O (85%)	0.1	98.9	99.6
TS-1	H_2O	0.1	46.8	93.3
	t-BuOH/H_2O (85%)	0.1	66.2	92.4
	t-BuOH/H_2O (85%)	0.3	96.5	99.3

[a]Ammoximation conditions: cyclohexanone, 20 mmol; ketone:H_2O_2:NH_3 = 1:1.2:1.5 (molar ratio); solvent, 12 g; temp., 333 K; time, 2 h.

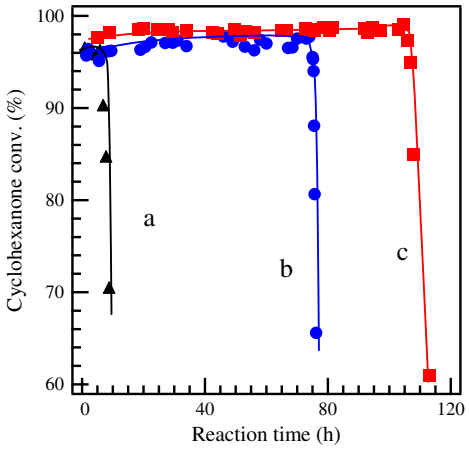

Fig. 11. The lifetime of TS-1 (a), Ti-MOR (b), and Ti-Meso-MOR (c) in the ammoximation of cyclohexanone in a continuous slurry reactor. Ammoximation conditions: cat., 1.6 g; ketone:H_2O_2:NH_3 = 1:1.1:1.7 (molar ratio); ketone feeding rate, 21.8 mL h^{-1}; temp., 333 K; solvent, *t*-BuOH (85 wt.%).

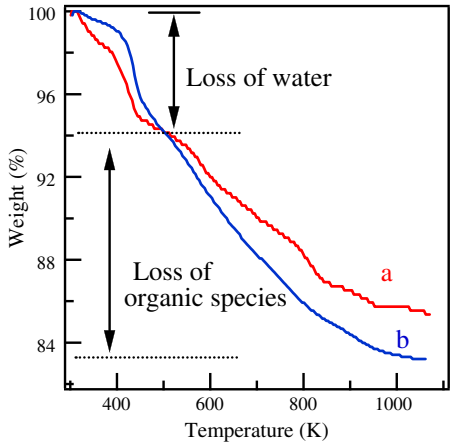

Fig. 12. TG curves of Ti-Meso-MOR (a) and Ti-MOR (b) after being used in continuous ammoximation for 107 h and 75 h, respectively.

catalytic properties in a continuous reaction is more important from a practical point of view. Thus, the lifetime of Ti-Meso-MOR was investigated in a slurry bed reactor, which is usually used to evaluate the quality and usability of commercial catalysts of TS-1 [54]. This so-called mandatory deactivation method is to check the duration of titanosilicate until ketone conversion below 95% using a determined catalyst loading, while the reactants and solvent are fed continuously into the reactor. Fig. 11 compares the lifetime among three kinds of titanosilicates under the same conditions. The oxime selectivity was always higher than 99% when the ketone conversion was over 95%. The lifetime of TS-1 lasted for only 8 h after that the ketone conversion dropped sharply due to deactivation (Fig. 11a). Ti-MOR deactivated at 75 h (Fig. 11b), showing a much longer lifetime than TS-1. Ti-Meso-MOR, on the other hand, possessed the longest lifetime of 107 h (Fig. 11c), which again can be ascribed to the advantage of mesopores.

The deactivation of titanosilicates in ammoximation has been previously investigated to be caused mainly by coke formation and partially by framework desilication in basic reaction mixture [54]. Thus, we have characterized the used catalysts. First, we have checked the crystalline structure of the recovered Ti-Meso-MOR after being used in ammoximation for 107 h. The XRD patterns indicated that the catalyst almost maintained the MOR structure (Fig. S2). The crystallinity of recovered catalyst was about 94% of the fresh one. This implies that a structural degradation occurred slightly probably because of desilication in basic reaction media. Nevertheless, the structural collapse was not significant. The ICP analysis indicated that the used Ti-Meso-MOR catalyst had a Si/Ti ratio of 92 in comparison with the ratio of 99 for the fresh one. This means the absolute Ti content in catalyst increased after ammoximation. We have observed very similar phenomena in the case of Ti-MWW-catalyzed ammoximation [54]. Different from hydroxylation and epoxidation, the ammoximation operated in basic media causes the desilication of titanosilicates easily.

UV–vis spectra were measured to check possible change in coordination states of the Ti species. After ammoximation, the recovered catalyst without calcination still showed the main band at 220 nm due to tetrahedral Ti species (Fig. S3b). A shoulder band at 260 nm probably due to the coordination of NH_3 was also observed. However, after calcination in air at 773 K for 5 h, the recovered catalyst showed a UV–vis spectrum very similar to that of fresh one (Fig. S3c). The catalytic activity of thus regenerated catalyst has been investigated in batchwise ammoximation of cyclohexanone. Under the same reaction conditions as fresh Ti-Meso-MOR (85% *t*-BuOH as solvent, other conditions see Table 2), the regenerated catalyst showed 94.6% cyclohexanone conversion and 99.3% oxime selectivity. Comparing with the conversion of 97.7% achieved with fresh Ti-Meso-MOR, a slight deactivation was observed. Nevertheless, considering the fact that the catalyst survived a long run in ammoximation, we suggest that Ti-Meso-MOR was relatively stable and regenerable.

The heavy byproducts accumulated gradually with process time and deposited inside the channels of titanosilicates, which may block the Ti active sites wherein. Ti-Meso-MOR, characteristic of mesoporosity, is considered to afford enough space for the diffusion of H_2O_2 and NH_3 molecules into the channels. Actually, TG analysis indicated that the used Ti-Meso-MOR catalyst contained about 8.7 wt.% organic species, which showed a weight loss in a wide temperature range (400–800 K) (Fig. 12a). We have demonstrated that they corresponded to the heavy byproducts formed in ammoximation system, including cyclohexanecarboxamide, 2-cyclohexylcyclohexanone, *N*-cyclohexylidenecyclohexanamine, and ε-caprolactam [54]. On the other hand, the weight loss due

to heavy organic species reached 10.2 wt.% on the recovered Ti-MOR catalyst irrespective of a shorter life in ammoximation (75 h) (Fig. 12b). Thus, the mesopores are helpful to minimize diffusion limitation and suppress coke formation efficiently, which then leads to a longer catalytic life with Ti-Meso-MOR.

4. Conclusion

MOR-type titanosilicate containing mesopores has been successfully postsynthesized by a combination of acid, alkaline, and $TiCl_4$ vapor treatments. A controlled alkaline treatment on partially dealuminated mordenite can cause a framework desilication and create the mesopores simultaneously, while the crystalline structure is well preserved. Tetrahedral Ti species are possibly inserted into the framework of mesoporous dealuminated mordenite mainly through the reaction of $TiCl_4$ molecules with the silanol groups on defect sites. The mesopores interconnect with 12-MR micropores, which enhance the accessibility to the active sites inside pores. The mesopore formation can minimize the diffusing limitation and depress the cock formation as well. Ti-Meso-MOR is superior to conventional Ti-MOR and TS-1 in toluene hydroxylation. Moreover, the porosity improvement endows Ti-Meso-MOR with high catalytic efficiency and duration in the cyclohexanone ammoximation either in a batch-type reactor or in a continuous slurry reactor, implying it could be a potential catalyst for clean production of oximes.

Acknowledgments

We gratefully acknowledge the NSFC of China (20890124, 20925310, and 20873043), the Science and Technology Commission of Shanghai Municipality (09XD1401500), and the Shanghai Leading Academic Discipline Project (B409).

Appendix A. Supplementary material

Supplementary data associated with this article can be found, in the online version, at doi:10.1016/j.jcat.2011.05.009.

References

[1] G. Bellussi, M.S. Rigguto, Stud. Surf. Sci. Catal. 137 (2001) 911–920.
[2] P. Ratnasamy, D. Srinivas, H. Knözinger, Adv. Catal. 48 (2004) 1–169.
[3] G. Bellussi, C. Perego, in: G. Ertl, H. Knozinger, J. Weitkamp (Eds.), Handbook of Heterogeneous Catalysis, vol. 5, Wiley, Poiters, 1997, p. 2329.
[4] (a) Eur. Chem. News 6 (1995) 23.;
(b) P.R. Saronno, M.P. Milan, et al., US 4745221, 1988.;
(c) P. Roffia, G. Leofanti, A. Cesana, M. Mantegazza, M. Padovan, G. Petrini, S. Tonti, P. Gervasutti, Stud. Surf. Sci. Catal. 55 (1990) 43–52.
[5] H. Ichihashi, H. Sato, Appl. Catal. A 221 (2001) 359–366.
[6] T. Yashima, Y. Kobayashi, T. Komatsu, S. Namba, Stud. Surf. Sci. Catal. 75 (1993) 1689–1692.
[7] .P. Wu, T. Komatsu, T. Yashima, J. Phys. Chem. B 102 (1998) 9297–9303.
[8] M. Reichinger, W. Schmidt, M.W.E. Van de Berg, A. Aerts, J.A. Martens, C.E.A. Krischhock, H. Gies, W. Grünert, J. Catal. 269 (2010) 367–375.
[9] (a) G. Bellussi, A. Carati, M.G. Clerici, G. Maddinelli, R. Millini, J. Catal. 133 (1992) 220–230;
(b) M.G. Clerici, P. Ingallina, J. Catal. 140 (1993) 71–83.
[10] (a) P. Wu, T. Tatsumi, T. Komatsu, T. Yashima, J. Phys. Chem. B 105 (2001) 2897–2905;
(b) P. Wu, T. Tatsumi, T. Komatsu, T. Yashima, J. Catal. 202 (2001) 245–255.
[11] A. Corma, M.A. Camblor, P.A. Esteve, A. Martínez, J. Pèrez-Pariente, J. Catal. 145 (1994) 151–158.
[12] A. Tuel, Zeolites 15 (1995) 236–242.
[13] P. Wu, T. Komastu, T. Yashima, J. Phys. Chem. 100 (1996) 10316–10322.
[14] A. Corma, U. Diaz, M.E. Domine, V. Fornes, J. Am. Chem. Soc. 122 (2000) 2804–2809.
[15] P. Wu, D. Nuntasri, J.F. Ruan, Y.M. Liu, M.Y. He, W.B. Fan, O. Terasaki, T. Tatsumi, J. Phys. Chem. B 108 (2004) 19126–19131.
[16] S.Y. Kim, H.J. Ban, W.S. Ahn, Catal. Lett. 113 (2007) 160–164.
[17] P. Wu, J.F. Ruan, L.L. Wang, L.L. Wu, Y. Wang, Y.M. Liu, W.B. Fan, M.Y. He, O. Terasaki, T. Tatsumi, J. Am. Chem. Soc. 130 (2008) 8178–8187.
[18] I.E. Maxwell, W.H.J. Stork, in: H.V. Bekkum, E.M. Flanigen, J.C. Jonsen (Eds.), Introduction to zeolite Science and Practise, Elsevier, Amsterdam, 1991, p. 71.
[19] P. Wu, T. Komastu, T. Yashima, J. Phys. Chem. B 102 (1998) 9297–9303.
[20] K.H. Chung, Micropor. Mesopor. Mater. 111 (2008) 544–550.
[21] F. Jin, Y. Tian, Y.D. Li, Ind. Eng. Chem. Res. 48 (2009) 1873–1879.
[22] Y. Tao, H. Kanoh, K. Kaneko, J. Am. Chem. Soc. 125 (2003) 6044–6045.
[23] M. Choi, H.S. Cho, R. Srivastava, C. Venkatesan, D.H. Choi, R. Ryoo, Nat. Mater. 5 (2006) 718–723.
[24] D.P. Serrano, J. Aguado, J.M. Escola, J.M. Rodriguez, A. Peral, J. Mater. Chem. 18 (2008) 4210–4218.
[25] M. Reichinger, W. Schmidt, M.W.E. van den Berg, A. Aerts, J.A. Martens, C.E.A. Kirschhock, H. Gies, W. Grünert, J. Catal. 269 (2010) 367–375.
[26] K. Na, M. Choi, W. Park, Y. Sakamoto, O. Terasaki, R. Ryoo, J. Am. Chem. Soc. 132 (2010) 4169–4177.
[27] J. Pérez-Ramírez, C.H. Christensen, K. Egeblad, C.H. Christensen, J.C. Groen, Chem. Soc. Rev. 37 (2008) 2530–2542.
[28] H. Wang, T.J. Pinnavaia, Angew. Chem. Int. Ed. 45 (2006) 7603–7606.
[29] B. Zhang, S.A. Davis, S. Mann, Chem. Mater. 14 (2002) 1369–1375.
[30] L. Tosheva, V. Valtchev, J. Sterte, Micropor. Mesopor. Mater. 35–36 (2000) 621–629.
[31] H.Q. Yang, Q. Liu, Z.C. Liu, H.X. Gao, Z.K. Xie, Micropor. Mesopor. Mater. 127 (2010) 213–218.
[32] A. Čižmek, B. Subotic, I. Smit, A. Tonejc, A. Rosario, F. Crea, A. Nastro, Micropor. Mater. 8 (1997) 159–169.
[33] X.L. Zhu, L.L. Lobban, R.G. Mallinson, D.E. Resasco, J. Catal. 271 (2010) 88–98.
[34] J.C. Groen, G.M. Hamminga, J.A. Moulijna, J. Pérez-Ramírez, Phys. Chem. Chem. Phys. 9 (2007) 4822–4830.
[35] J.C. Groen, J.C. Jansen, J.A. Moulijn, J. Pérez-Ramírez, J. Phys. Chem. B 108 (2004) 13062–13065.
[36] A.N.C. van Laak, S.L. Sagala, J. Zečević, H. Friedrich, P.E. de Jongh, K.P. de Jong, J. Catal. 276 (2010) 170–180.
[37] K.P. de Jong, J. Zečević, H. Friedrich, P.E. de Jongh, M. Bulut, S. van Donk, R. Kenmogne, A. Finiels, V. Hulea, F. Fajula, Angew. Chem. Int. Ed. 49 (2010) 10074–10078.
[38] J.C. Groen, S. Abelló, L.A. Villaescusa, J. Pérez-Ramírez, Micropor. Mesopor. Mater. 114 (2008) 93–102.
[39] X. Wei, P.G. Smirniotis, Micropor. Mesopor. Mater. 97 (2006) 97–106.
[40] L. Sommer, D. Mores, S. Svelle, M. Stöker, B.M. Weckhuysen, U. Olsbye, Micropor. Mesopor. Mater. 132 (2010) 384–394.
[41] P. Wu, T. Komatsu, T. Yashima, J. Phys. Chem. 99 (1995) 10923–10931.
[42] J.C. Groen, T. Sano, J.A. Moulijn, J. Pérez-Ramírez, J. Catal. 251 (2007) 21–27.
[43] M.G. Clerici, G. Bellussi, U. Romano, J. Catal. 129 (1991) 159–167.
[44] M. Ogura, S. Shinomiya, J. Tateno, Y. Nara, M. Nomura, E. Kikuchi, M. Matsukata, Appl. Catal. A 219 (2001) 33–43.
[45] K.-H. Lee, B.-H. Ha, Micropor. Mesopor. Mater. 23 (1988) 211–219.
[46] G. Bellussi, M.S. Rigguto, Stud. Surf. Sci. Catal. 85 (1994) 177–213.
[47] K. Segawa, H. Tachibana, J. Catal. 131 (1991) 482–490.
[48] J.T. Miller, P.D. Hopkins, B.L. Meyers, G.J. Ray, R.T. Roginski, G.W. Zajac, N.H. Rosenbaum, J. Catal. 138 (1992) 115–128.
[49] P. Wu, K. Komatsu, T. Yashima, Stud. Surf. Sci. Catal. 105 (1997) 663–670.
[50] (a) L. Davies, P. McMorn, D. Bethell, P.C.B. Page, F. King, F.E. Hancock, G.J. Hutchings, Chem. Commun. 18 (2000) 1807–1808;
(b) L. Davies, P. McMorn, D. Bethell, P.C.B. Page, F. King, F.E. Hancock, G.J. Hutchings, Phys. Chem. Chem. Phys. 3 (2001) 632–639.
[51] A. Thangaraj, S. Sivasanker, P. Ratnasamy, J. Catal. 131 (1991) 394–400.
[52] F. Song, Y.M. Liu, H.H. Wu, M.Y. He, P. Wu, T. Tatsumi, J. Catal. 237 (2006) 359–367.
[53] P. Wu, T. Komatsu, T. Yashima, J. Catal. 168 (1997) 400–411.
[54] S. Zhao, X. Wei, J.X. Yang, Y.M. Liu, Y.T. Zhang, B.L. Xu, J.G. Jiang, H.M. He, P. Wu, Appl. Catal. A 394 (2011) 1–8.